Preprint Title	Photochemical synthesis of Silver Nanoprisms via green LEDs irradiation and evaluation of SERS activity
Authors	Tuan Anh Mai-Ngoc, Nhi Kieu Vo, Cong Danh Nguyen, Thi Kim Xuan Nguyen and Thanh Sinh Do
Publication Date	15 Mai 2025
Article Type	Full Research Paper
Supporting Information File 1	AgNPrs-SERS BJNANO manucrispt_ Sup.docx; 1.3 MB
ORCID® iDs	Tuan Anh Mai-Ngoc - https://orcid.org/0009-0004-5860-6969

Photochemical synthesis of Silver Nanoprisms via green LEDs irradiation and evaluation of SERS activity

Tuan Anh Mai-Ngoc[1*], Nhi Kieu Vo[1], Cong Danh Nguyen[1], Thi Kim Xuan Nguyen[1] and Thanh Sinh Do[1]

[1]Nanotechnology Lab, Research Laboratories of Saigon Hi-Tech Park, Lot I3, N2 Street, Tan Phu Ward, Ho Chi Minh City 70000, Vietnam

Email: anhmnt.shtplabs@gmail.com

Abstract

Silver nanoprisms (AgNPrs) are promising candidates for surface-enhanced Raman scattering (SERS) due to their strong localized surface plasmon resonance (LSPR) and sharp-tip geometry. In this study, AgNPrs were synthesized through a photochemical method by irradiating spherical silver nanoparticle seeds with 10W green LEDs (520 ± 20 nm) for various durations up to 72 hours. The growth mechanism was investigated through UV–Vis spectroscopy, FE-SEM, XRD and TEM analyses, confirming the gradual transformation of spherical seeds into AgNPrs. Optimal conversion was observed after 72 hours of irradiation, producing well-defined AgNPrs with an average size of 78 nm. The SERS activity of the AgNPrs was evaluated using 4-mercaptobenzoic acid (4-MBA) as a probe molecule. Compared to spherical AgNPs, AgNPrs exhibited a significantly higher SERS enhancement factor (EF), calculated as 1.15×10^6, enabling detection limits down to 10^{-9} M. These findings demonstrate that green LED-mediated synthesis provides a simple, environmentally friendly route to fabricate high-yield AgNPrs with superior SERS capabilities, suitable for ultrasensitive chemical and biological sensing applications.

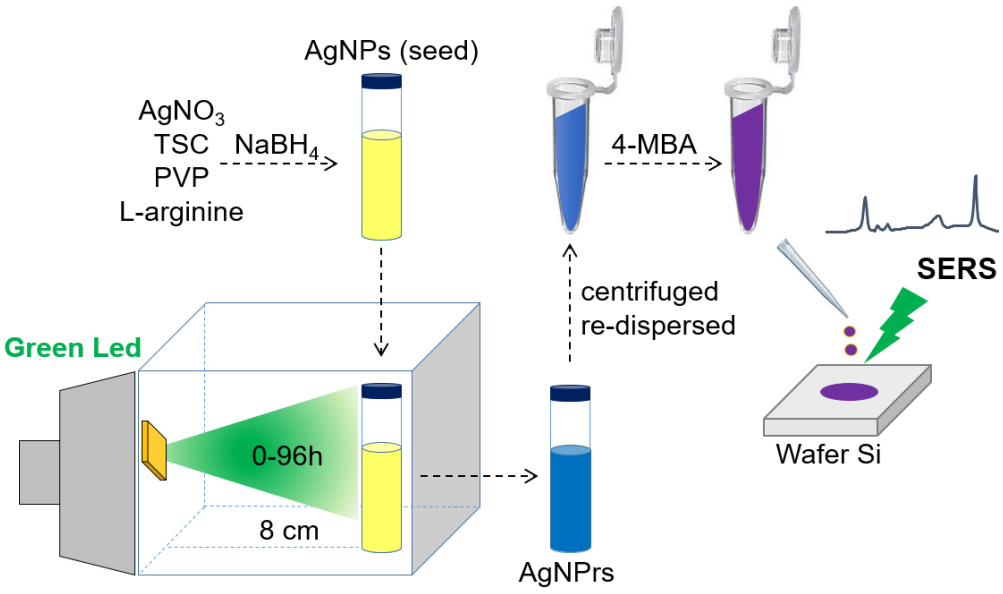

Graphical abstract

Keywords:

photochemical synthesis, LEDs, silver nanoprisms, surface-enhanced Raman scattering (SERS), trisodium citrate

Introdution

Anisotropic silver nanoparticles (ASNPs) have attracted increasing attention from research groups worldwide due to their potential applications in optical sensing, particularly in surface-enhanced Raman scattering (SERS) [1]. Among ASNPs, silver nanoprisms (AgNPrs) are of particular interest because of their broad absorption in the visible range (400–900 nm), enabling them to display a wide spectrum of colors such as yellow, red, orange, violet, green, and blue. This makes AgNPrs highly suitable for optical sensing applications [2].

The formation mechanism of AgNPrs in solution typically proceeds through three stages: nucleation, seeding, and crystallization, with the crystallization phase being the slowest and rate-determining step of the entire process [3]. During this stage, small silver nanoparticles (seeds) can combine and evolve into anisotropic nanostructures through a chemical reduction process in the presence of hydrogen peroxide (H_2O_2), as a shape controlling agent, commonly referred to as the Mirkin method [4]. Recently, photochemical methods utilizing physical agents such as lasers [5], UV light [6], or LEDs [7,8] have gained attention due to their superior spatial and temporal control, high stability of the resulting AgNPrs and avoidance of environmentally unfriendly reducing agents [8,9].

Trisodium citrate (TSC) plays a crucial role in protection the face crystal (111) of the silver crystal structure and is thus essential in the formation of ASNPs. Our previous study have shown that a molar ratio R = [TSC]/[Ag^+] = 5 favors the formation of silver nanoprisms, whereas R = 25 promotes the formation of silver nanodecahedrons (AgNDs) [10].

The strong surface plasmon resonance (SPR) exhibited by AgNPrs significantly contributes to SERS enhancement by amplifying local electromagnetic fields. This makes AgNPrs ideal candidates for SERS-based sensing applications [1]. Numerous studies have focused on the fabrication of SERS-active substrates by depositing AgNPrs onto various solid supports such as glass [11], quartz, silicon, or aluminum foil [12]. A recent trend in the development of practical SERS substrates emphasizes flexibility and portability for field-deployable Raman detection. Accordingly, several groups have developed paper-based [13] or cotton-based [14] SERS substrates by impregnating them with silver nanostructures. While many efforts have been devoted to the synthesis of AgNPrs and evaluation of their SERS activity, limited studies have focused on the SERS performance of photochemically synthesized AgNPrs, particularly in 4-mercaptobenzoic acid (4-MBA) as a probe molecule.

In this study, AgNPrs were synthesized via a photochemical fabrication using green LED 10W irradiation. Seeds were prepared using 1 mM $AgNO_3$ and stabilized with a TSC:$AgNO_3$ molar ratio of 5. Physicochemical analyses confirmed the successful formation of AgNPrs with high yield. The SERS performance of the synthesized

AgNPrs, evaluated using 4-MBA as a probe molecule, demonstrated significantly enhanced Raman signals compared to the initial AgNPs seeds, highlighting their potential applicability in SERS-based sensors.

Results and Discussion

Synthesis of seeds

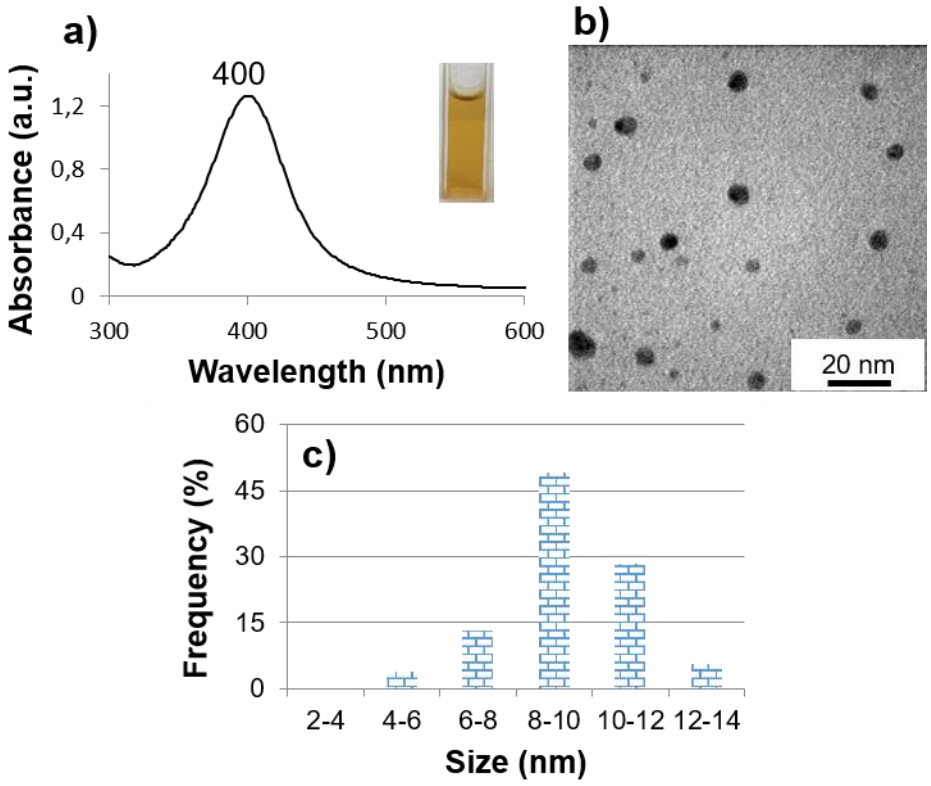

Figure 1: (a) UV-Vis spectrum, (b) TEM image and (c) size distribution of seeds

The UV-Vis spectra of the AgNPs seed shown in the Figure 1a displayed a single peak at 400 nm, indicating the presence of spherical silver nanoparticles with small sizes, consistent with studies in the literature [4,6,7]. The sample exhibited the characteristic yellow color of AgNPs. The TEM image and size distribution in the Figure 1b,c showed that the seed predominantly contained spherical silver nanoparticles with a size of approximately 10 nm, in agreement with the UV-Vis spectrum result.

Manufacturing of AgNPrs

AgNPrs were synthesized in 2 steps: (i) synthesis of AgNPs as seeds and (ii) irradiating the seeds with green LEDs to form AgNPrs with the aid of L-A [10]. Due to the different SPR properties between AgNPs and AgNPrs, the morphological transformation of silver nanostructures in sample can be observed through UV-Vis spectra in Figure 2.

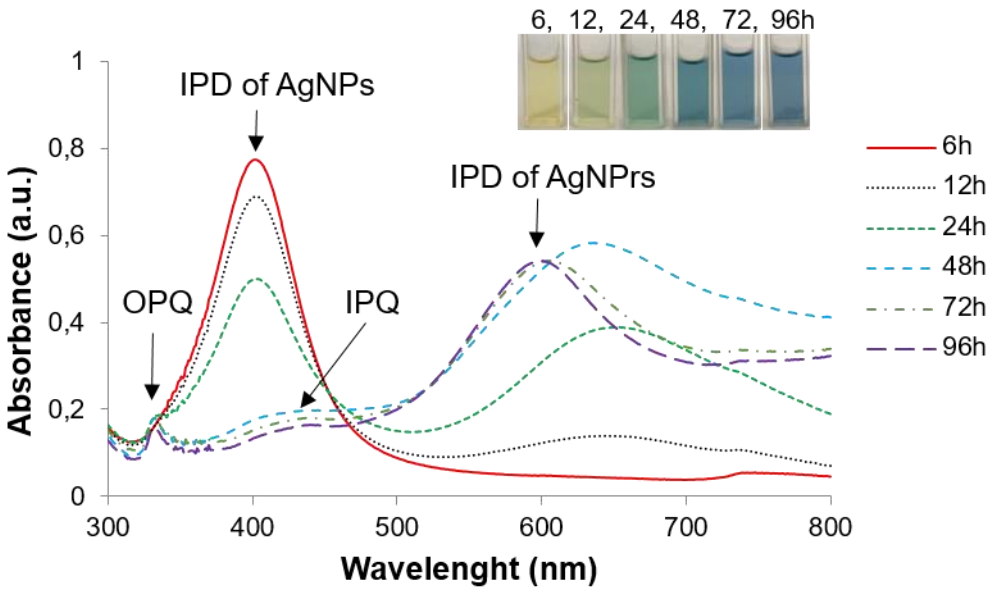

Figure 2: UV-Vis spectra of silver nanoparticles at different LED irradiation times.

After 6 hours of LED irradiation, the UV–Vis spectrum exhibited a single absorption peak at 402 nm, characteristic of the in-plane dipole (IPD) resonance of spherical silver nanoparticles. The solution retained its yellow color, indicating that the seed morphology remained largely unchanged and that no formation of anisotropic silver nanostructures had occurred at this stage [4,7]. The IPD peak was still observed at 12 and 24 hours but with progressively decreasing intensity, suggesting a reduction in the number of spherical silver seeds as the irradiation time increased.

At 12 hours, in addition to the spherical IPD peak at 405 nm, a broad shoulder began to emerge at approximately 650 nm. This shoulder became more prominent at 24 hours, shifting slightly to 662 nm. The appearance of this absorption feature in the longer wavelength region indicated the onset of anisotropic nanoparticle formation, such as silver nanoprisms [4,5,6,7].

After 48 hours of LED irradiation, the IPD peak associated with spherical nanoparticles disappeared entirely. Instead, the UV–Vis spectrum displayed three distinct absorption peaks: (i) an out-of-plane quadrupole (OPQ) peak at 333 nm, indicative of the nanoplate thickness; (ii) an in-plane quadrupole (IPQ) peak at 440 nm with weak intensity; and (iii) a strong in-plane dipole (IPD) peak at 654 nm, characteristic of silver nanoprisms. The simultaneous presence of these three plasmonic modes, along with the disappearance of the spherical IPD peak, confirmed that the seeds had largely transformed into silver nanoplates after 48 hours of LED irradiation.

Moreover, the IPD peak showed a noticeable blue shift. Previous studies have shown that the position of the IPD peak is closely correlated with the edge-to-thickness ratio of the nanoprisms [4,15]. Therefore, the clear observation of the OPQ peak at 48 hours suggests a significant contribution of nanoplate thickness to the overall surface plasmon resonance behavior, which could account for the blue shift of the IPD peak.

At 72 and 96 hours, the OPQ and IPQ peaks remained stable at 333 nm and 440 nm, respectively, indicating that the transformation of silver seeds into nanoplates had

reached equilibrium. The IPD peak continued to blue-shift slightly (to 604 nm and 600 nm, respectively), but no significant changes were observed in the overall UV–Vis spectral profiles. Based on these results, we conclude that 72 hours represents the optimal irradiation time for the complete transformation of silver seeds into silver nanoplates in this study.

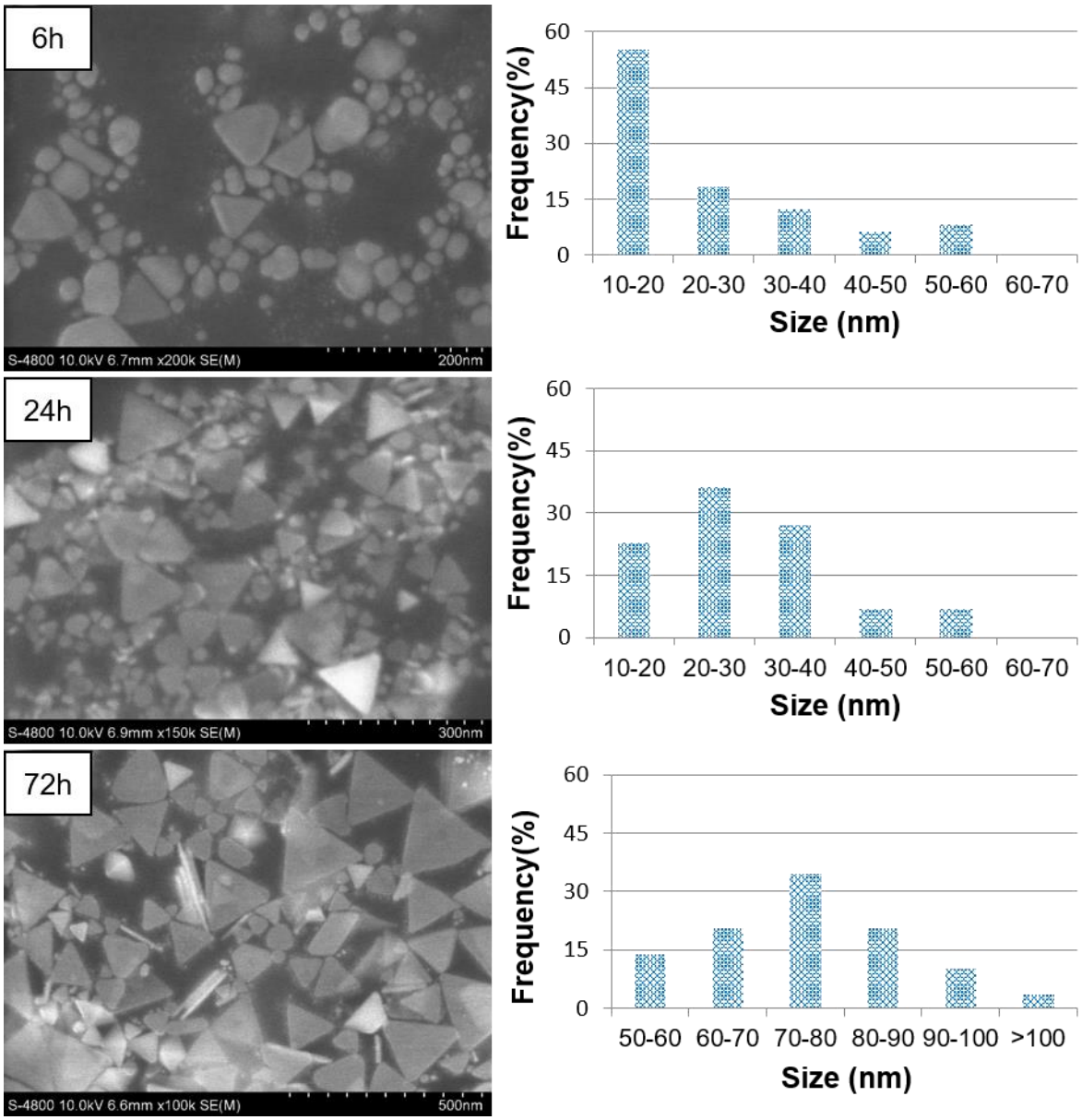

Figure 3: FE-SEM images and size distribution of silver nanoparticles after 6, 24 and 72 hours of LED irradiation.

From the FE-SEM images and particle size distribution graph after 12 hours of LED irradiation in Figure 3, it is observed that the particle sizes are primarily concentrated in the 10–20 nm range, which corresponds to spherical silver nanoparticles. Additionally, some particles with larger sizes around 35–40 nm were also present; these could be AgNPrs or round silver nanoplates, although their number was minimal. This indicates that after 12 hours, the sample mainly consists of spherical silver

nanoparticles, while nanoplates have started to form but remain scarce. These FE-SEM results are consistent with the UV-Vis spectra discussed previously.

Upon increasing the irradiation time to 48 hours, the particle sizes became larger compared to the 12h sample, predominantly in the range of 25–35 nm, suggesting a greater presence of AgNPrs. However, the persistence of AgNPs and round silver nanoparticles implies that the conversion efficiency from AgNPs to AgNPrs remains relatively low.

At 72 hours of LED irradiation, the particle size increased significantly compared to the 12h and 48h samples, mostly ranging between 70 - 80 nm. At this stage, the majority of particles are identified as AgNPrs. Only a negligible number of sAgNPs and round silver nanoplates remain. The average size of the AgNPrs at this stage is 78 nm, approximately double that of the 12h and 48h samples. It can thus be concluded that 72 hours is the optimal duration for the transformation of AgNPs into AgNPrs using green LED irradiation, aligning well with the UV-Vis spectroscopy results.

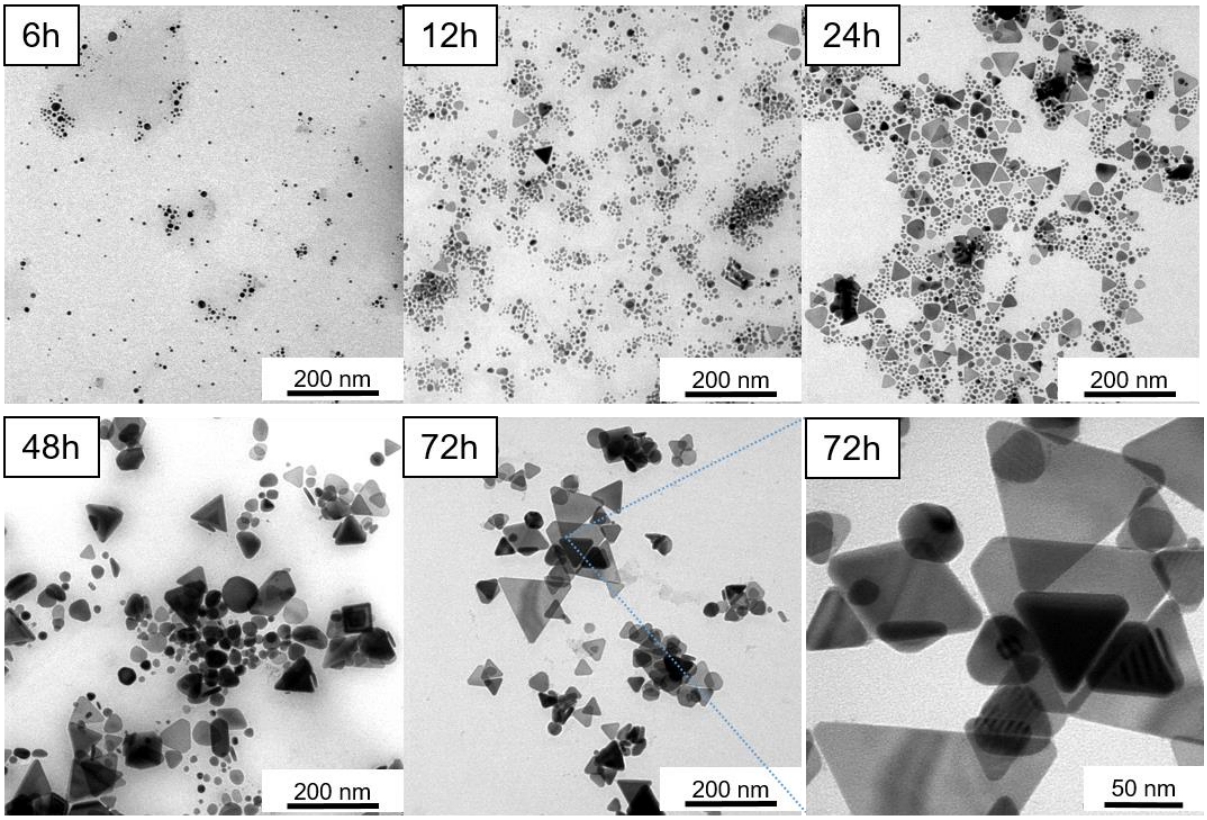

Figure 4: TEM images of silver nanoparticles after 12, 24, 48, and 72 hours of LED irradiation.

TEM images of the samples at a magnification of 50,000 after 6, 12, 24, 48, and 72 hours of LED irradiation are shown in Figure 4. The results indicate that after 6 hours, the sample predominantly contained spherical silver nanoparticles. As the LED irradiation time increased, the proportion of AgNPrs became more significant. At 24 hours, both AgNPs and AgNPrs coexisted, which is consistent with the UV–Vis spectrum showing two distinct IPD peaks corresponding to each morphology.

After 48 hours, AgNPs - seeds were no longer visibly present in significant amounts; the sample was mainly composed of AgNPrs. This observation correlates with the appearance of the OPQ peak, characteristic of nanoplate thickness, and the disappearance of the IPD peak of AgNPs in the UV–Vis spectrum. By 72 hours, TEM images showed exclusively AgNPrs, which were clearly visible and well-defined, in agreement with the corresponding FE-SEM images.

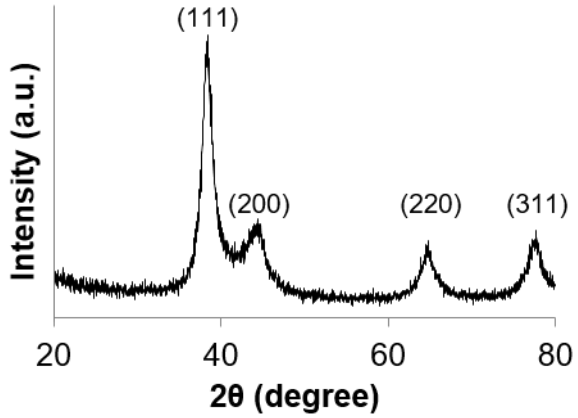

Figure 5: XRD spectrum of AgNPrs after 72 hours of LED irradiation

The XRD spectrum of AgNPrs after 72 hours of LED irradiation (Figure 5) exhibited four distinct broad diffraction peaks at 38.2°, 44.3°, 64.5°, and 77.7°, corresponding to the (111), (200), (220), and (311) crystal planes, respectively. These peaks are characteristic of the face-centered cubic (fcc) structure of silver nanoparticles. The diffraction intensity at the (111) crystal face was three times higher than that at the (200), consistent with the typical structure of AgNPrs [10,16]. Moreover, no diffraction peaks corresponding to Ag_2O were detected, indicating that the photoreduction process for synthesizing AgNPrs was efficient.

In summary, after 72 hours of LED irradiation under the experimental conditions, small spherical silver nanoparticles - seeds had been almost completely converted into silver nanoprisms. Unlike conventional chemical synthesis methods, the photochemical LED-based approach does not produce fragmented or etched structures, resulting in well-formed AgNPrs. Additionally, this method avoids excessive oxidative–reductive agents such as H_2O_2, thereby improving the structural integrity, stability, and potential applicability of the resulting AgNPrs.

Formation mechanism of AgNPrs

During the seed development process leading to the formation of AgNPrs, two critical components play decisive roles: the source of silver ions (Ag^+) and the reducing agent that converts Ag^+ to metallic silver (Ag^0).

Upon LED irradiation of the system containing initial AgNPs seeds, the atomic layers of silver at the nanoparticle surfaces are excited and oxidized by dissolved oxygen in the solution, generating Ag^+ ions [15]. These ions serve as the source of Ag^+ for the seed growth process. Trisodium citrate (TSC) preferentially binds to the (111) crystal facets of silver nanoparticles. Under LED illumination, TSC is excited and oxidized, acting as a reducing agent through the following reactions:

Citrate + hν → Acetone-1,3-dicarboxylate + CO_2 + $2e^-$ (1)

$Ag^+ + e^- \rightarrow Ag^0$ (2)

Electrons released from TSC immediately reduce Ag^+ to Ag^0. Since the (111) facets are protected by TSC, the newly formed Ag^0 preferentially deposits on the (100) and (110) surfaces, leading to planar two-dimensional growth and the formation of planar twinned seeds [6,7]. Subsequently, as LED irradiation continues, the surfaces of the silver nanomaterials (initial AgNPs seeds, planar twinned seeds) are continuously excited, and the growth of AgNPrs proceeds via two mechanisms (Figure 6):

- Mechanism 1: TSC continues to be excited and promotes the reduction of Ag^+, resulting in the deposition of Ag^0 on the edges of small AgNPrs, thereby increasing their edge lengths over time [7,10,16].

- Mechanism 2: Instead of further edge growth, small AgNPrs can laterally attach to one another. At the junctions, Ag^+ is reduced by TSC under LED stimulation, facilitating their fusion and leading to the formation of larger AgNPrs with approximately double the original edge length [16,17].

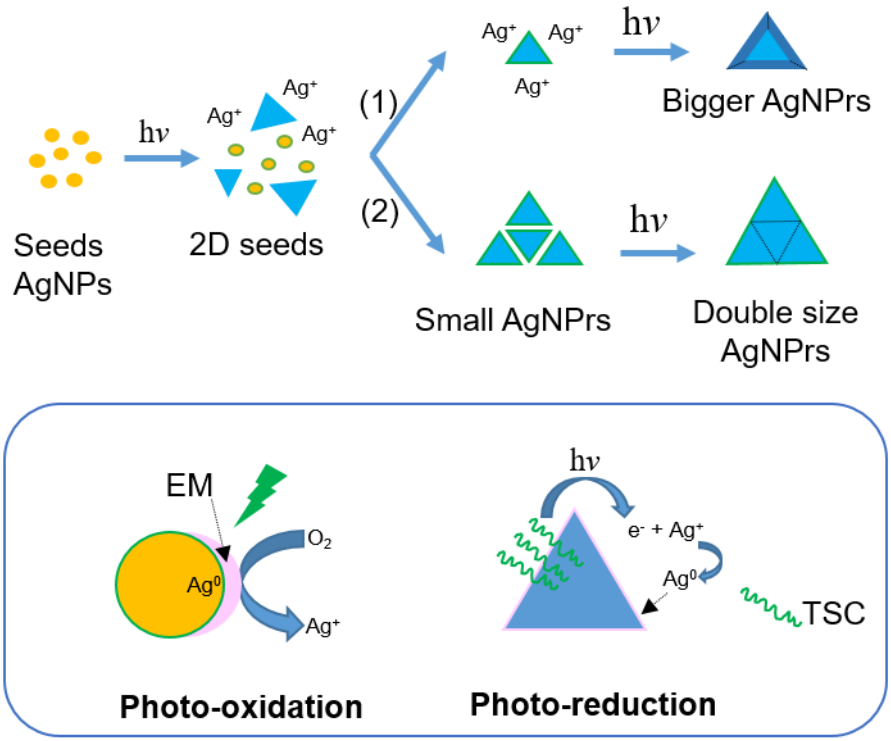

Figue 6: Mechanisms proposed for AgNPrs formation

In the current study, the high precursor concentration (1 mM $AgNO_3$) likely promoted frequent interparticle collisions. Initially, AgNPrs formed via mechanism 1 and grew to approximately 40 nm in size. Subsequently, these smaller AgNPrs underwent edge-to-edge fusion, yielding larger AgNPrs with edge lengths exceeding 80 nm, consistent with mechanism 2.

In summary, TSC plays a crucial role in guiding crystal growth: it binds to the (111) surfaces, releases electrons upon LED excitation, drives the reduction of Ag^{+}, and promotes the deposition of Ag^{0} on unprotected facets, thereby facilitating two-dimensional growth and the formation of AgNPrs.

SERS properties of silver nanoparticles

In this study, 4-mercaptobenzoic acid (4-MBA) was used as the probe molecule due to its widely use in both intrinsic and extrinsic SERS applications [18,19]. It exhibits strong affinity toward silver nanoparticles via Ag–S bonding, which significantly enhances the SERS signal. Additionally, the carboxylic acid (–COOH) group of 4-MBA readily enables further functionalization with other compounds, making it suitable for biosensing applications.

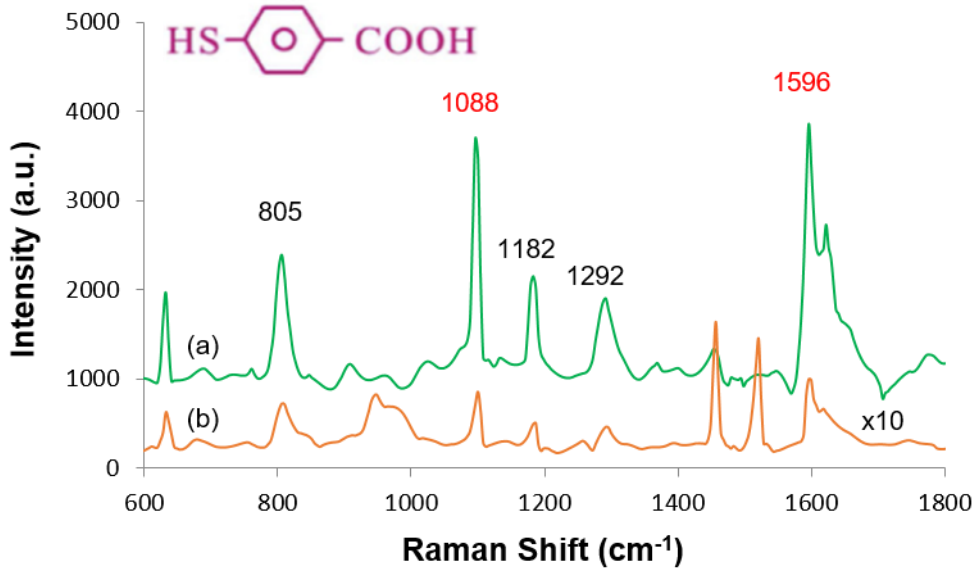

Figure 7: Raman spectra of (a) solid 4-MBA and (b) 4-MBA (10^{-1} M, amplified 10-fold)

The Raman spectrum of solid 4-MBA (Figure 7, curve a) displays two dominant peaks at 1088 cm^{-1} and 1596 cm^{-1}, corresponding to the stretching vibrations of the aromatic ring. Weaker peaks are observed at 1182 cm^{-1} and 1292 cm^{-1}, attributed to C–H stretching, and at 805 cm^{-1}, corresponding to the bending vibration of the carboxylate group (COO^{-}) [20,21]. The Raman spectrum of a 100 mM 4-MBA solution, recorded on a Si wafer and amplified 10-fold (Figure 7, curve b), also shows the 1088 cm^{-1} and 1596 cm^{-1} peaks with lower intensity, consistent with literature reports at the same concentration and excitation wavelength of 532 nm [20].

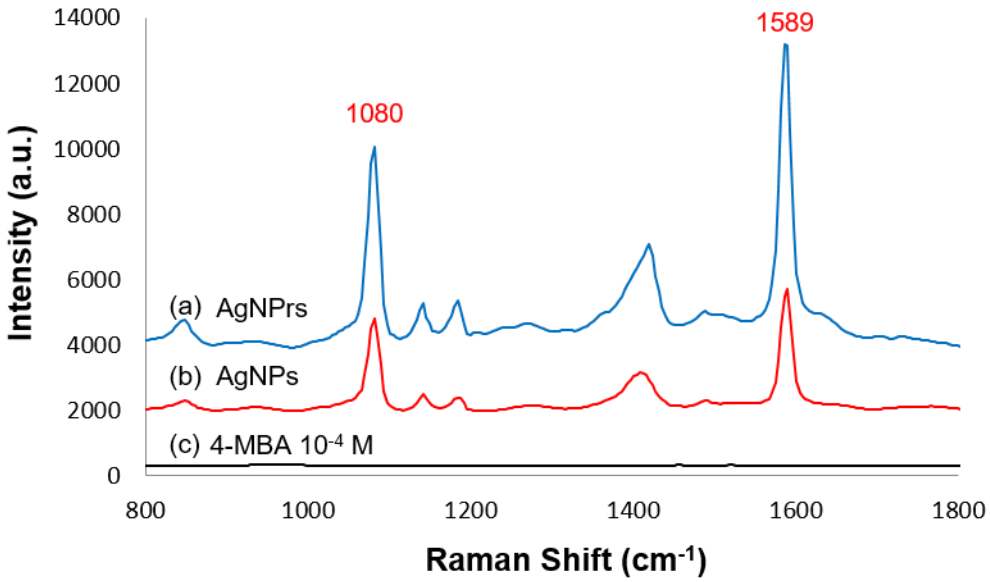

Figure 8: Raman spectra of the mixture of 4-MBA (10^{-5} M) and (a) AgNPrs (after 72 hours of LED irradiation) or (b) AgNPs (seeds) and (c) 4-MBA 10^{-4} M.

It is evident that the Raman spectrum of 4-MBA at 10^{-4} M (Figure 8, curve c) shows no detectable peaks, whereas the SERS spectra of 4-MBA at 10^{-5} M, enhanced by both AgNPs ((Figure 8, curve b) and AgNPrs (Figure 8, curve a), exhibit strong signals at 1080 cm^{-1} and 1589 cm^{-1}, corresponding to aromatic ring vibrations. Additional weaker peaks at 1148 cm^{-1} and 1184 cm^{-1} are assigned to C–H stretching modes [21,22]. These findings demonstrate the SERS-enhancing capability of the silver nanomaterials synthesized in this study.

The SERS enhancement effect of each nanomaterial was evaluated based on the intensity of the 1589 cm^{-1} peak. Overall, AgNPrs exhibited significantly stronger SERS activity compared to AgNPs (seeds). The enhancement factor (EF) was calculated using equation (3) [23]:

$$EF = \frac{I_{SERS}.N_{bulk}}{I_{bulk}.N_{SERS}} \qquad (3)$$

where I_{SERS} and I_{bulk} are the Raman intensities of 4-MBA in the presence and absence of silver nanomaterials, respectively. N_{SERS} and N_{bulk} are the number of 4-MBA molecules excited by the laser in the SERS and non-SERS conditions, respectively. Since the same volume (20 µL) and method were used, N_{SERS} and N_{bulk} can be substituted by C_{SERS} and C_{blank}, corresponding to the concentrations of 4-MBA [22]. In this study, $C_{blank} = 10^{-1}$ M and $C_{SERS} = 10^{-5}$ M. Based on this equation, the enhancement factors for AgNPrs and AgNPs were calculated to be 1,15 $x10^{6}$ and 4,2 $x10^{5}$, respectively. These results confirm that AgNPrs exhibited superior SERS performance, consistent with prior studies investigating the direct SERS detection of 4-MBA [18,19].

Due to their anisotropic structure, AgNPrs concentrate surface electrons and form electromagnetic “hot spots” at the edges and tip of the nanoprisms [22,24,25]. These

hot spots significantly enhance the local electric field, thereby improving SERS efficiency relative to isotropic spherical nanoparticles. For AgNPrs, hot spots at the tip and edges play a key role in SERS enhancement, while the flat surfaces contribute less effectively [25]. Consequently, AgNPrs with triangular sharp, well-defined vertices exhibit better SERS properties than round-edged or poorly defined nanoplate structures.

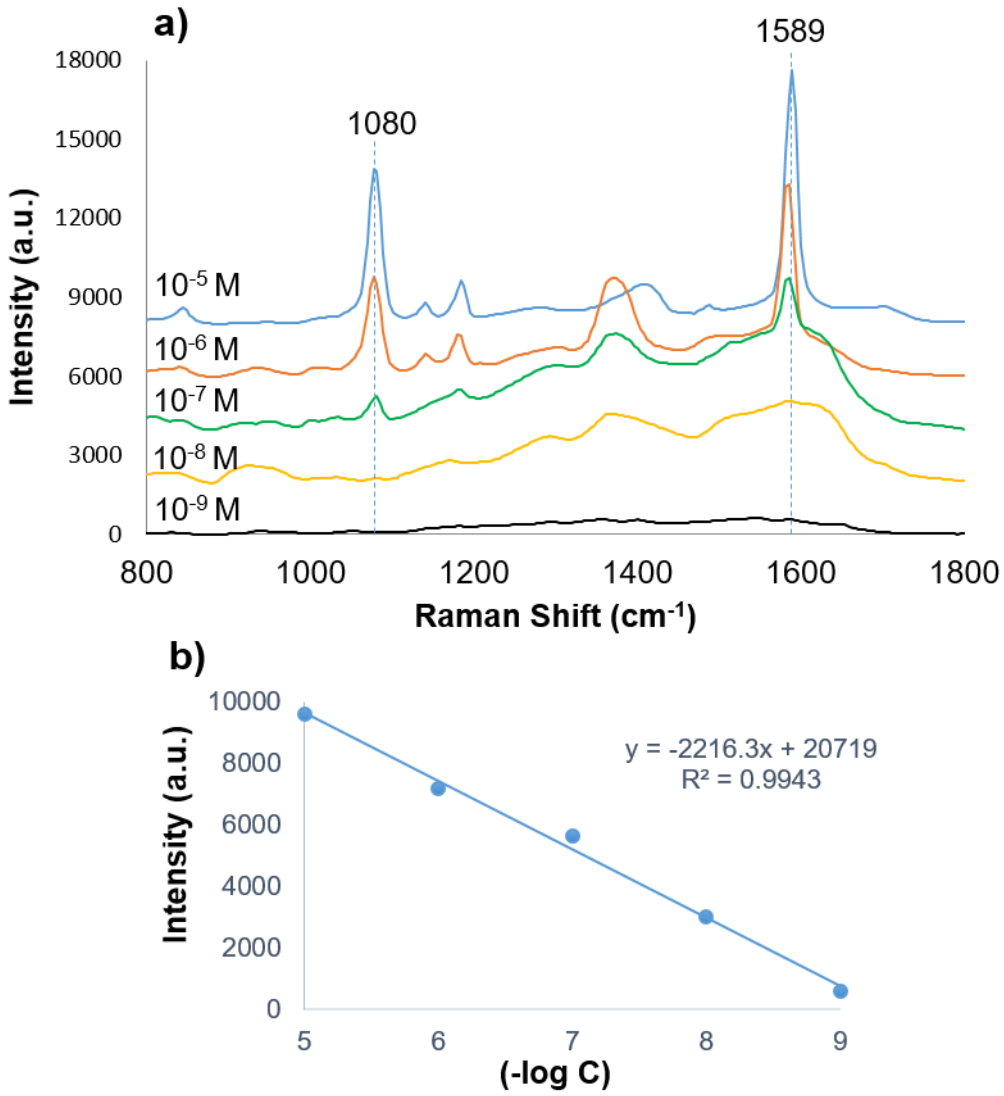

Figure 9: (a) Raman spectra of the mixture of AgNPrs and 4-MBA with various concentration and (b) The relationship between the intensity of peak at 1589 cm^{-1} versus the concentration of 4-MBA in the range from 10^{-9} M to 10^{-5} M.

To further evaluate sensitivity, Raman spectra of mixture of AgNPrs and 4-MBA with various concentration at concentrations ranging from 10^{-5} M to 10^{-9} M were recorded. As shown in Figure 9a, the peak at 1589 cm^{-1} gradually decreased in intensity with decreasing concentration. Even at 10^{-7}M, the peak remained clearly observable. At 10^{-8} M and 10^{-9} M, the peak intensity was still detectable but less well-defined. This is likely due to the fixed quantity of AgNPrs across all experiments, while the concentration of 4-MBA decreased logarithmically. Since the sample was prepared by

drop-casting onto a Si wafer, AgNPrs tended to aggregate, which may have led to reduced resolution of the Raman peaks at very low analyte concentrations.

The relationship between 4-MBA concentration and the intensity of the 1589 cm^{-1} peak (Figure 9b) was found to be linear, following the equation y = -2216,3x + 20719, R^2=0,9943. This linear correlation indicates that the lowest 4-MBA concentration detectable with this AgNPr-based SERS substrate was 10^{-9} M, confirming its potential for ultrasensitive SERS-based sensing applications.

Conclusion

This study demonstrates a facile, eco-friendly photochemical method for synthesizing AgNPrs using green LED irradiation without the need for harsh chemical reagents. The transformation of AgNPs seeds into AgNPrs was confirmed through UV–Vis, FE-SEM, and TEM analyses, with optimal formation achieved at 72 hours of irradiation. The resulting AgNPrs showed significantly enhanced SERS performance compared to spherical AgNPs, attributed to the anisotropic morphology and formation of electromagnetic hot spots at the nanoplate tips and edges. Using 4-MBA as a Raman probe, the AgNPr-based SERS substrate enabled detection at concentrations as low as 10^{-9} M with a strong linear response. These results highlight the potential of LED-synthesized AgNPrs as high-performance, low-cost, and environmentally benign substrates for sensitive SERS applications in chemical and biosensing fields.

Experimental

Chemical

Silver nitrate (AgNO3, >99%), trisodium citrate tribasic dihydrate (TSC, >99%), 4-mercapto benzoic acid (4-MBA, 99%) were obtained from Sigma-Aldrich, Darmstadt, Germany. L-arginine (L-A, 99%), sodium borohydride (NaBH4, 98%) were obtained from Merck, Darmstadt, Germany. Polyvinylpyrrolidone (PVP K30) were purchased from Prolabo, Kennersburg, NJ, USA. Chemicals were used without any purification. Deionized (DI) water with a resistance of 18 MΩ cm (Milli-Q) was used in all the experiments. All glasswares were cleaned with aqua regia before use.

Synthesis of seeds

A total of 10 mL of 0.05 M trisodium citrate (TSC), 300 µL of 0.05 M polyvinylpyrrolidone (PVP), 20 mL of 5 mM $AgNO_3$, and 500 µL of 0.005 M L-arginine solution were added into a beaker. Deionized water was then added to adjust the total volume of the solution to 100 mL. The mixture was magnetically stirred at 500 rpm for 5 minutes. Subsequently, 1.6 mL of 100 mM sodium borohydride ($NaBH_4$) solution (cooling with ice) was rapidly injected using a micropipette. The solution was stirred for an additional 30 minutes, during which the color of the mixture changed from colorless to dark yellow, then to bright yellow, and finally to a lighter yellow. The solution was stirred at room temperature and aged in the dark overnight.

Manufacturing of AgNPrs

A volume of 20 mL of the seed solution was transferred into 25 mL glass vials (Wheaton, Germany). These vials were placed vertically at a fixed distance of 8 cm from the LED light source, inside a cardboard box internally lined with aluminum foil. The LEDs were oriented perpendicularly to the vials to ensure that each vial was consistently positioned at the center of the incident light beam throughout all experiments. The seed solutions were irradiated with green LEDs (520 ± 20 nm, Epistar 10W chip, Taiwan) for 6, 12, 24, 48, and 72 hours. During the irradiation process, the color of the solution gradually shifted from pale yellow to green and eventually to blue.

Characterization

The optical properties of the samples were characterized using UV–Vis spectroscopy (Jasco V-670) with a scanning range from 900 nm to 200 nm. Samples were diluted tenfold with deionized water prior to measurement.

To determine the morphology, particle size of the synthesized nanostructures, the samples were analyzed using field emission scanning electron microscopy (FE-SEM, Hitachi S-4800, Japan) and transmission electron microscopy (TEM, JEM-1400, Japan). For TEM analysis, a droplet of the nanoparticle dispersion was deposited onto a 3 mm copper grid and allowed to dry at room temperature. For FE-SEM analysis, the dried sample was mounted on conductive carbon tape and imaged at an accelerating voltage of 10 kV. TEM imaging was performed at an accelerating voltage of 100 kV.

The structure of the AgNPrs was analyzed by X-ray diffraction (XRD) using a D8 Advance-Bruker instrument equipped with a Cu-Kα radiation source (40 kV, 40 mA) at a scanning rate of 4°/min.

SERS Measurement

The SERS properties of the AgNPs and AgNPrs were investigated on a Si wafer surface with the 4-MBA raman reporter. The Si wafer was cut to a size of 1x1 cm, was treated with piranha solution (H_2SO_4:H_2O_2 = 3:1) before used to remove organic compounds. A 2 mL sample was centrifuged at 12,000 rpm for 15 minutes, with the supernatant discarded, and the solid residue was re-dispersed in 1 mL of distilled water. 50 µL of 10^{-4} M 4-MBA solution was added to 450 µL of the re-dispersed sample and left for 1 hour at room temperature. 20 µL of the resulting mixture was placed on the Si wafer substrate, allowed to dry at room temperature, and Raman measurements were performed (HORIBA XploRA ONE TM, France) using a 532 nm laser source and a 10x magnification microscope. Measurements were taken at 10 random positions, and the average intensity was recorded.

Funding

This study was funded by the People's Committee of Ho Chi Minh City, performed with the support of the Board of Management of Saigon High-Tech Park (SHTP) and Research Laboratory of Saigon Hi-Tech Park (SHTPLABs).

References

[1] Wang, Y.; Schlucker, S. *Analyst*, **2013**, *138(8)*, 2224-2238. https://doi.org/10.1039/C3AN36866A

[2] Kordasht, H. K.; Bahavarnia, P.; Bahavarnia, F.; Hasanzadeh, M.; Shadjou, N. *RSC Advances*, **2025,** *15(7*), 5105-5116. https://doi.org/10.1039/D4RA08469A

[3] Chen, Y.; Fan, Z.; Zhang Z.; Niu W.; Li C.; Yang N.; Chen B.; Zhang, H*. Chem Rev*, **2018,** *118(13)*, 6409–6455. https://doi.org/10.1021/acs.chemrev.7b00727

[4] Métraux, G. S.; Mirkin, C. A. *Advanced Materials*, **2005**, 17, 412-415. https://doi.org/10.1002/adma.200401086

[5] Mahar, N.; Al-Saadi, A. A. *Spectrochimica Acta Part A: Molecular and Biomolecular Spectroscopy,* **2023***,* 302, 122996. https://doi.org/10.1016/j.saa.2023.122996

[6] Gunawardana, N.; Ke, C-Y.; Huang, C-L.; Yang C-H. *Optical Materials*, **2024**, 148, 114932. https://doi.org/10.1016/j.optmat.2024.114932

[7] Saade, J.; Araújo, C. B. *Materials Chemistry and Physics*, **2014**, 148, 1184-1193. https://doi.org/10.1016/j.matchemphys.2014.09.045

[8] Anh, M. N. T.; Nguyen, D. T. D.; Thanh, N. V. K.; N.T.P. Phong, D.H. Nguyen, M-T. Nguyen-Le. *Processes*, **2020**, 8(3), 292-299. https://doi.org/10.3390/pr8030292

[9] Furletov, A. A.; Apyari, V. V.; Zaytsev, V. D.; Sarkisyan, A. O.; Dmitrienko, S. G. *Trends in Analytical Chemistry,* **2023***,* 166, 117202. https://doi.org/10.1016/j.trac.2023.117202

[10] Anh, M. N. T.; Nguyen, C. D.; Vo, N. K.; Ngo, V.K.T.; Nguyen, T. P. P; Nguyen, D. H. *Vietnam Journal of Catalysis and Adsorption*, *2021*, 10, 270-274. https://doi.org/10.51316/jca.2021.142

[11] Li, K.; Jiang, K.; Zhang, L.; Wang, Y.; Mao, L.; Zeng, J.; Lu, Y.; Wang P. *Nanotechnology*, **2016**, 27, 165401-165407. https://doi.org/10.1088/0957-4484/27/16/165401

[12] Jana, D.; Mandal, A.; De, G., *ACS Applied Materials & Interfaces*, **2012**, 4, 3330-3334. https://doi.org/10.1021/am300781h

[13] Restaino, S.M.; White I. M. *Analytica Chimica Acta*, **2018**, 1060, pp. 17-29. https://doi.org/10.1016/j.aca.2018.11.057

[14] Cheng, D.; He, M.; Ran, J.; Cai, G.; Wu, J.; Wang, X. *Sensors & Actuators: B. Chemical*, **2018**, 270, 508–517. https://doi.org/10.1016/j.snb.2018.05.075

[15] Scardaci, V. *Nanomaterials*, **2021**, 11, 2226. https://doi.org/10.3390/nano11092226

[16] Ashkarran A. A. *Optical Materials*, **2016**, 58, 454-460. https://doi.org/10.1016/j.optmat.2016.06.037

[17] Xue, C.; Metraux, G. S.; Millstone, J. E.; Mirkin, C. A. *Journal of the American Chemical Society*, **2008**, 130, 8337-8344. https://doi.org/10.1021/ja8005258

[18] Chattopadhyay, S.; Sabharwal, P. K.; Jain, S.; Kaur, A.; Singh, H. *Analytica Chimica Acta*, **2019**, 1067, 98-106. https://doi.org/10.1016/j.aca.2019.03.050

[19] Hu, S-S.; Qiao, S.; Pan, J-B.; Kang, B.; Xu, J-J.; Chen, H-Y. *Talanta*, **2018**, 179, 9-14. https://doi.org/10.1016/j.talanta.2017.10.038

[20] Ma, W.; Fang, Y.; Hao, G.; Wang, W. *Chinese Journal of Chemical Physics*, **2010**, 23(6), 659-663. https://doi.org/10.1088/1674-0068/23/06/659-663

[21] Marques, F .C. ; Alves, R. S. ; Santos ,D.P.; Andrade, G. F. S. *Physical Chemistry Chemical Physics*, **2022**, 24, 27449-27458. https://doi.org/10.1039/D2CP03375E
[22] Yan, J.; Han, X.; He, J.; Kang, L.; Zhang, B.; Du, Y.; Zhang, H.; Dong, C.; Wang, H-L.; Xu, P., *ACS Applied Materials & Interfaces*, **2012**, 4, 2752-2756. https://doi.org/10.1021/am300381v
[23] Jiang, L.; You, T.; Yin, P.; Shang, Y.; Zhang, D.; Guo, L.; Yang, S. *Nanoscale*, **2013**, 5, 2784-2789. https://doi.org/10.1039/C3NR33502J
[24] Zannotti, M.; Rossi, A.; Giovannetti, R. *Coatings*, **2020**, 10(3), 288-299. https://doi.org/10.3390/coatings10030288
[25] Zhang, C-H.; Zhu, J. ; Li, J-J.; Zhao, J-W. *ACS Applied Materials & Interfaces*, **2017**, 9(20), 17387-17398. https://doi.org/10.1021/acsami.7b04365